[CANCER RESEARCH 61, 6413–6422, September 1, 2001]

Mechanisms Associated with Tumor Vascular Shut-Down Induced by Combretastatin A-4 Phosphate: Intravital Microscopy and Measurement of Vascular Permeability[1]

Gillian M. Tozer,[2] Vivien E. Prise, John Wilson, Maja Cemazar, Siqing Shan, Mark W. Dewhirst, Paul R. Barber, Borivoj Vojnovic, and David J. Chaplin

Gray Cancer Institute, Mount Vernon Hospital, Northwood, Middlesex, HA6 2JR, United Kingdom [G. M. T., V. E. P., J. W., M. C., P. R. B., B. V., D. J. C.], and Department of Radiation Oncology, Duke University Medical Center, Duke University, Durham, North Carolina [S. S., M. W. D.]

ABSTRACT

The tumor vascular effects of the tubulin destabilizing agent disodium combretastatin A-4 3-*O*-phosphate (CA-4-P) were investigated in the rat P22 tumor growing in a dorsal skin flap window chamber implanted into BD9 rats. CA-4-P is in clinical trial as a tumor vascular targeting agent. In animal tumors, it can cause the shut-down of blood flow, leading to extensive tumor cell necrosis. However, the mechanisms leading to vascular shut-down are still unknown. Tumor vascular effects were visualized and monitored on-line before and after the administration of two doses of CA-4-P (30 and 100 mg/kg) using intravital microscopy. The combined effect of CA-4-P and systemic nitric oxide synthase (NOS) inhibition using N^{ω}-nitro-L-arginine (L-NNA) was also assessed, because this combination has been shown previously to have a potentiating effect. The early effect of CA-4-P on tumor vascular permeability to albumin was determined to assess whether this could be involved in the mechanism of action of the drug. Tumor blood flow reduction was extremely rapid after CA-4-P treatment, with red cell velocity decreasing throughout the observation period and dropping to <5% of the starting value by 1 h. NOS inhibition alone caused a 50% decrease in red cell velocity, and the combined treatment of CA-4-P and NOS inhibition was approximately additive. The mechanism of blood flow reduction was very different for NOS inhibition and CA-4-P. That of NOS inhibition could be explained by a decrease in vessel diameter, which was most profound on the arteriolar side of the tumor circulation. In contrast, the effects of CA-4-P resembled an acute inflammatory reaction resulting in a visible loss of a large proportion of the smallest blood vessels. There was some return of visible vasculature at 1 h after treatment, but the blood in these vessels was static or nearly so, and many of the vessels were distended. The hematocrit within larger draining tumor venules tended to increase at early times after CA-4-P, suggesting fluid loss from the blood. The stacking of red cells to form rouleaux was also a common feature, coincident with slowing of blood flow; and these two factors would lead to an increase in viscous resistance to blood flow. Tumor vascular permeability to albumin was increased to ~160% of control values at 1 and 10 min after treatment. This could lead to an early decrease in tumor blood flow via an imbalance between intravascular and tissue pressures and/or an increase in blood viscosity as a result of increased hematocrit. These results suggest a mechanism of action of CA-4-P *in vivo*. Combination of CA-4-P with a NOS inhibitor has an additive effect, which it may be possible to exploit therapeutically.

INTRODUCTION

Most tumor cells rely on an intact vascular supply for their survival, making the tumor vasculature an attractive target for therapy (1, 2). Development of antiangiogenic strategies for cancer therapy is an active area of research, with several classes of agents, such as inhibitors of vascular endothelial growth factor and inhibitors of matrix metalloproteinases, now in clinical trial. In contrast to the antiangiogenesis approach, antivascular approaches aim to target the established tumor vasculature, causing a rapid and extensive decrease in tumor blood flow, which leads to secondary tumor cell death. Vascular-targeted gene therapy and the use of antibodies to specific epitopes on the tumor vasculature are two possible ways of achieving this, the accessibility of endothelial cells to blood-borne vectors making this an attractive alternative to targeting the tumor cells themselves. In addition, the tumor vasculature has been shown to be particularly sensitive to two main classes of low-molecular weight drugs, *i.e.*, the tubulin-binding agents (3), and drugs related to flavone acetic acid, such as dimethylxanthenone-acetic acid (4).

The tubulin-binding agents, vincristine and vinblastine, are well-established cytotoxic drugs that have also been found to cause extensive vascular damage in animal tumors at close to their maximum tolerated doses (5). The tubulin-binding agent, colchicine, was found to produce hemorrhagic necrosis in human tumors, but toxicity prevented its further development (6). CA-4-P,[3] which is cleaved to its active form, CA-4, by endogenous, nonspecific phosphatases, is one of a number of compounds isolated from the South African bush willow tree, *Combretum caffrum* (7, 8). CA-4 has a high affinity for tubulin at or near the colchicine binding site (9) and, like colchicine, causes the destabilization of the tubulin cytoskeleton. This results in extensive tumor vascular damage and necrosis in transplanted (ectopic and orthotopic) and spontaneous tumors (10–13). However, unlike colchicine, it can have these effects at relatively nontoxic doses (14). It was shown recently that blood flow rate to a s.c. transplanted rat tumor decreased rapidly, to almost undetectable levels, by 6 h after i.p. treatment with 100 mg/kg CA-4-P, whereas the blood-flow rate to normal tissues was much less affected (15). In addition, it was found that systemic NOS inhibition using N^{ω}-nitro-L-arginine methyl ester potentiated the effect in tumor tissue but not in normal tissues (15). This finding links the mechanism of action of CA-4-P to that of other vascular-damaging strategies, such as photodynamic therapy and ischemia-reperfusion injury, the effects of which have also been enhanced by NOS inhibition (16, 17). A significant increase in vascular resistance was also obtained in tumors perfused *ex vivo* with a cell-free perfusate, although the effect was much less than that observed *in vivo* (15). *In vitro* studies have shown that endothelial cells are particularly sensitive to the effects of CA-4-P compared with various other cell types (18). Proliferating human umbilical vein endothelial cells round up when exposed to CA-4-P (13, 19), and this is associated with condensation of the tubulin and reorganization of the actin cytoskeletons and increased permeability of an endothelial cell monolayer to macromolecules (18). The time course of these changes is very similar to the CA-4-P-induced vascular effects in *ex vivo* perfused tumors (15), suggesting that endothelial cell shape change and

Received 9/13/00; accepted 7/2/01.

The costs of publication of this article were defrayed in part by the payment of page charges. This article must therefore be hereby marked *advertisement* in accordance with 18 U.S.C. Section 1734 solely to indicate this fact.

[1] This work was supported by the Cancer Research Campaign, the National Lottery Charities Board of the United Kingdom, and a travel grant from NATO (to M. W. D.).

[2] To whom requests for reprints should be addressed, at the Gray Cancer Institute, P. O. Box 100, Mount Vernon Hospital, Northwood, Middlesex, HA6 2JR, United Kingdom. Phone: 44-01923-828611; Fax: 44-01923-835210; E-mail: tozer@graylab.ac.uk.

[3] The abbreviations used are: CA-4-P, disodium combretastatin A-4 3-*0*-phosphate; NO, nitric oxide; L-NNA, N^{ω}-nitro-L-arginine; NOS, nitric oxide synthase; ROI, region of interest; MABP, mean arterial blood pressure.

an increase in vascular permeability may be related to the vascular effects of CA-4-P observed *in vivo*.

CA-4-P has the potential for combination with conventional cytotoxic agents and radiotherapy (14, 20, 21), and Phase I clinical trials of CA-4-P as a single agent are near completion in the United Kingdom and the United States. However, more mechanistic information is needed to optimize treatment with CA-4-P and to develop more effective analogues of the drug. The aims of the current study were: (*a*) to extend our understanding of the vascular effects of CA-4-P by direct microscopic observation of tumor blood vessels, subsequent to treatment, in a rat window chamber model; (*b*) to administer CA-4-P with and without systemic NOS inhibition to clarify the role of nitric NO production in the CA-4-P-induced vascular effects; and (*c*) to determine whether CA-4-P treatment causes a change in tumor vascular permeability *in vivo*.

MATERIALS AND METHODS

Window Chamber Surgery. All animal experiments were carried out in accordance with the United Kingdom Animals (Scientific Procedures) Act 1986 and with approval from the Ethical Review Committee of the Gray Cancer Institute, Northwood, United Kingdom. Surgery was carried out under general anesthesia using i.p. injection of fentanyl citrate (0.32 mg/kg) and fluanisone (10 mg/kg; Hypnorm; Janssen Animal Health) and midazolam (5 mg/kg; Hypnovel; Roche, Welwyn Garden City, United Kingdom). Animals were kept warm using heated pads throughout the surgical procedure, and aseptic technique was used throughout. Window chambers, consisting of a double-sided aluminum frame holding two parallel glass windows ~200 μm apart, were surgically implanted into the dorsal skin of male BD9 rats weighing ~200 g. Surgery involved removing the epidermal and dermal layers of both skin layers of a dorsal skin flap, except for the deepest fascia layer on each side, and then securing the two sides of the chamber to the skin using stainless steel screws and sutures (22, 23). After this procedure, the two fascia layers moved freely between the two glass windows. Early-generation s.c. transplants of the P22 rat carcinosarcoma (24) were used as donor tumors. Tumor fragments (~0.5 mm in diameter) were placed onto one of the fascia layers, within the window chamber, immediately following surgery. Animals were given a s.c. injection of a few ml of dextrose-saline immediately after surgery and kept on a warmed pad until recovery from anesthesia. Subsequently, animals were kept in a warm room, 32–34°C, until the day of the experiment.

Marker Red Cells. Donor red cells were obtained by cardiac puncture from anesthetized male BD9 rats into a heparinized syringe and fluorescently labeled with DiI (D-282 Molecular Probes; Cambridge Bioscience) for the measurement of red cell velocity and flux in recipient animals. This method has been published previously (25, 26). Briefly, labeling consisted of separating red cells from plasma and other cellular constituents by centrifugation and incubating the washed red cells with DiI for 30 min at room temperature. Approximately 25 μg of DiI were used per 50 μl of packed red cells. After incubation, red cells were washed twice and resuspended in PBS to a concentration of 50 μl of DiI-labeled red cells/ml. Labeled cells were kept for up to 3 days at 4°C before use. Viability and uniformity of labeling were checked by microscopy.

Intravital Microscopy. Intravital microscopy was carried out 7–14 days after surgery, when tumors measured 3.4 $\pm$ 0.2 mm in diameter (mean $\pm$ 1 SE for the whole group). An inverted Nikon Diaphot 200 fluorescence microscope with a stage modified in-house for taking rats, was used. Animals were anesthetized with Hypnorm and midazolam and placed on the stage such that the window chamber was located centrally above the objectives using locating screws. Rectal temperature was maintained between 35–37°C throughout the experiment using a thermostatically controlled heating pad beneath the rat and an infrared overhead lamp. MABP was monitored continuously via a pressure transducer connected to a cannulated tail artery.

CA-4-P (provided by OxiGene, Inc., Lund, Sweden) was administered i.p. at 30 or 100 mg/kg in a volume of 3 ml/kg, made up in 0.9% saline with a few drops of 5% Na_2CO_3. Thirty mg/kg CA-4-P (or the vehicle for the drug) was administered 15 min after a bolus i.v. injection of the NOS inhibitor, L-NNA, or the vehicle for L-NNA (water acidified with a few drops of 1 N HCl). NOS inhibition was continued throughout the experiment by supplementing the i.v. bolus dose of L-NNA (10 mg/kg in a volume of 3 ml/kg) with a continuous i.v. infusion of L-NNA (10 μg/kg/h in a volume of 100 μl/kg/h) starting immediately after the bolus dose.

Either the upper or lower surface of the tumors was investigated. The upper surface enables a large number of venules and capillaries to be monitored. The lower surface is adjacent to the fascia layer from which the tumor microcirculation develops and allows monitoring of the supplying arteriolar vessels and larger draining venules. Intravital microscopy of tumors was carried out before and after administration of CA-4-P, with and without systemic NOS inhibition. Preceding the start of each experiment, an aliquot of fluorescently labeled red cells (~0.2 ml) was injected i.v. Tumor preparations were alternately viewed under transmitted visible light for the subsequent measurement of vessel numbers and diameters and under fluorescence ϵ-illumination using a 100-W mercury arc lamp for the subsequent measurement of red cell flux and velocity under fluorescence conditions. Fluorescence was set up to excite and detect the emissions from the red cells labeled with DiI (550 and 565 nm, respectively). Before the administration of drugs, a tumor ROI, approximately half-way between the center and the periphery of the tumor, was selected, using the $\times$20 objective, to include a range of different-sized vessels (the high-power ROI). At each time point, this ROI was monitored for 30 s using transmitted light and then for 60 s using ϵ-illumination. In addition, the tumor was monitored on transmitted light at each time point using the $\times$4, $\times$10, and, where possible, $\times$40 objective. Most of the tumor was visible using the $\times$4 objective. In addition, at the beginning and end of each experiment, the whole tumor was examined under high-power transmitted light ($\times$20 objective) and under very low power ($\times$1.5 objective). Exposure to transmitted light and ϵ-illumination was limited to 90 s and 60 s, respectively, at each time point. XY stage micrometers could be used to return to a specific ROI (to within $<$10 μm) when required. Return to a specific focal plane within the ROI (Z direction) could be ensured by reference to specific vascular features within the field of view.

Data Analysis for Intravital Microscopy. Observations were recorded in a digital format, using a Sony DSR-30P digital videocassette recorder, for off-line analysis. Multiple frames (typically 10) were captured onto computer, and the images were averaged for the analysis of vessel numbers. Vessel numbers, rather than vessel density or length, were analyzed in order that each vessel could be described as "large" or "small" (see below) and so that the fate of individual vessels could be monitored. In all of the analyses, a single vessel was defined as a vessel length with no visible branches. No attempt was made to discriminate between small venules and true capillaries, where red cells proceed in single file, because of intermittent flow in some tumor vessels, which makes discrimination difficult. Therefore, venules were defined as being small or large if their diameters were $\leq$10 μm or $>$10 μm, respectively. Vessels on the lower surface of tumors were categorized as arterioles if they were narrow, fast-flowing, straight, with few branches, and with divergent flow afferent to the tumor. For analysis of vessel numbers, vessels were identified in images acquired before treatment, and these vessels were scored as being present or absent in subsequent images. Numbers of vessels, which were invisible in the images acquired before treatment but which appeared in subsequent images, were noted separately.

Image analysis software was developed in-house for the analysis of vessel numbers, combining automatic and manual vessel identification and counting. The software was written in the LabWindowsCVI 5.0 (National Instruments, Redmond, TX) environment to run under WindowsNT 4.0 (Microsoft Corporation). Working on the 10-frame-averaged images from a digital video cassette, the software performed image-processing functions to delineate the visible vessels and produce a skeleton "map" of vessels for each field from which the number of vessels was automatically counted. The algorithm performed image enhancement using spatial filters matched to vessel-like intensity profiles in two orthogonal orientations. These ridge-shaped spatial filters had a Gaussian profile with a width appropriate to approximate the transverse intensity profile of a vessel of known approximate diameter. They caused vessels to appear bright in the image, while suppressing all other structures. Hysteresis thresholding and skeletonization (27) were used to obtain a binary vessel map of connected 1-pixel-width lines automatically from the enhanced image. At this point, the operator could correct the map, if necessary, by observation. To determine vessel numbers, the points where vessels branch, cross, and "end" have to be identified within the vessel map. The end of a

vessel is normally where it progresses out of the plane of image focus. Although this was largely achieved automatically, the operator was required to intervene in cases where two very close branches and two vessels that cross but are not joined cannot be automatically distinguished. This often required reference to the taped video sequences. On average, the automated procedure correctly identified ~60% of the visible vessels, leaving the user to draw the remainder on screen using the computer mouse and custom user interface.

Additional analysis was carried out manually on all of the vessels in the higher power ROI (×20 objective) to identify functioning *versus* nonfunctioning vessels. Nonfunctioning vessels were defined as those vessels which had disappeared from the field of view (assessed by comparison of each image with the starting image) plus those vessels that contained stationary red cells for at least 30 s (the monitoring period for each time point).

Quantitative data on flow characteristics and diameter measurements were obtained from selected vessels within the high power ROI (×20 objective). Selection of four venules from the upper surface and up to four venules from the lower surface of tumors was based on examination of the pretreatment tapes. Vessels were chosen for their length (>30 μm, typically 100 μm), uniformity of flow, and a range of diameters within each tumor. Measurements were made with the aid of an image overlay hardware system (DAVID; Brian Reece Scientific Ltd., Reading, United Kingdom). This was calibrated using microscope distance standards (1, 10, and 100 μm) so that the distance between any pair of selected pixels could be directly read out, on the image, in microns. Diameters of selected venules on the upper and lower surfaces of tumors and of selected arterioles on the lower surface were measured. For these, pairs of points were chosen on opposite sides of the red cell column and perpendicular to it in each vessel (10 pairs/vessel) under transmitted visible light. Small vessels (<10 μm diameter) were not used for the diameter analysis. Measurement of the width of the red cell column may slightly underestimate the true vessel diameters. However, we were more interested in detecting changes in vessel diameter after treatment than in measuring absolute values, and we felt that the method chosen would be a reasonable reflection of this. In addition, alternative methods would have involved the use of exogenous fluorescent markers for identifying the vessel wall, and these may be vasoactive in themselves and can extravasate from hyperpermeable vessels leading to the obfuscation of vessel margins.

Red cell velocity and flux in all selected vessels were calculated from recorded data of the high-power ROI on fluorescence ϵ-illumination. At least 10 fluorescent red cells were monitored for velocity measurements over 60 s of recorded images. Velocity was calculated in μm/s from the number of video frames taken for each red cell to travel between two points of measured distance, marked on the vessel image. If, after treatment, no red cells were observed within the observation period, a value of 0.85 μm/s was assumed. This is a very small fraction of the average pretreatment velocity observed (see "Results") and represents the maximum possible velocity under this condition, assuming equal spacing of fluorescently labeled red cells. Using this method, there is a tendency to underestimate very slightly the degree of vascular shut-down observed. Changes in red cell flux were calculated from the number of fluorescent red cells crossing a single point marked on the vessel within a measured time (~1 min). On average, 57 fluorescent red cells/vessel were counted at the initial time point for the calculation of changes in red cell flux.

Flow rates through individual vessels on the upper surface were calculated from the red cell velocity and diameter measurements described above (flow rate = red cell velocity * π/4 *d^2), where d is vessel diameter. This assumes that the red cells are traveling with the bulk plasma flow. A few red cells, which were observed to be traveling slower than the majority within a particular vessel, were not used for velocity calculations. Relative changes in vascular resistance with time after treatment were estimated from the relative change in MABP divided by flow rate. Relative changes in hematocrit within individual vessels were calculated from changes in red cell flux relative to changes in the flow rate. That is, hematocrit α [red cell flux/(r^2 * red cell velocity)], where r is vessel radius. This approximates that treatment does not affect the mean volume of red cells, and that red cells travel with the bulk plasma flow.

Tumor Vascular Permeability to Albumin. For the measurement of changes in tumor vascular permeability to albumin at various times subsequent to CA-4-P treatment, the P22 carcinosarcoma was grown in the right inguinal fat pad of BD9 rats such that the tumor developed with only a single supplying artery and a single draining vein. This method has been published previously (28). Tumors were treated ~2 weeks after implantation (mean tumor weight ± SE was 0.59 ± 0.07 g for the whole group) and assayed after treatment with drug vehicle only (control) or 1, 10, 20, or 30 min after 30 mg/kg CA-4-P given i.p., as described above. Access to the tumor-supplying artery allowed changes in tumor vascular permeability to be determined via a slightly modified version of the classical Oldendorf method (29), originally used to determine changes in vascular permeability to various plasma solutes in the cerebral circulation. Briefly, at the assay time, an admixture of ~0.019 MBq (0.5 μCi) of the test compound (in this case, ^{125}I-labeled BSA; ICN Pharmaceuticals Ltd., Basingstoke, United Kingdom) and 0.008 MBq (0.2 μCi) of a low-molecular weight reference compound (in this case, ^{86}RbCl; Amersham Pharmacia Biotech UK Ltd., Little Chalfont, United Kingdom) was injected, in saline (0.1 ml), into the retrograde-cannulated saphenous artery. This meant that the admixture was washed directly into the tumor-supplying artery via arterial blood flow. Only a short time (10 s) was allowed to elapse, to minimize backflux into the vasculature and to ensure minimal recirculation, before the tumor was excised, weighed, and counted together with an injectate sample. Samples were counted on a Wallac Autogamma counter with suitable gating for the simultaneous assessment of counts from ^{125}I and ^{86}Rb. Because the admixture of tracers was administered directly to the tumor, the ratio of ^{125}I counts:^{86}Rb counts in the injectate was assumed to be equivalent to the ratio in the supplying blood. Therefore, any change in tumor vascular permeability to albumin subsequent to treatment was assessed by calculating the uptake of ^{125}I albumin into tumor tissue (^{125}I counts in tumor ÷ ^{125}I counts in injectate) as a percentage of the uptake of ^{86}RbCl (^{86}Rb counts in tumor ÷ ^{86}Rb counts in injectate). This tumor uptake index was considered to be a good index of changes in vascular permeability to BSA because the uptake of both tracers would be equally affected by blood flow changes after treatment, and the uptake of ^{86}RbCl is unlikely to be permeability-limited in tumors.

Statistics. Statistical analysis was carried out using JMP Statistics Version 3 for the Apple Macintosh (SAS Institute, Inc., Cary, NC). Intravital microscopy data were fitted to a multivariate model (MANOVA) with repeated measures to determine the effects of the different treatments on vessel numbers, diameters, MABP, red cell velocity, vascular resistance, and hematocrit over time. Responses were fitted to effects using least squares. The effect of variation between individual vessels was accounted for by using a nested design, and any variation between rats was described as random. Differences in responses caused by treatment or time were tested for significance using an approximate F test, based on comparison of the matrix for the hypothesis sum of squares and cross products with the matrix for the residual. Differences in response were described as significant if the probability corresponding to the F value was <0.05. The Student t test for unpaired data was used to test for significant differences in tumor uptake indices for different treatment groups. A $P < 0.05$ was considered significant.

RESULTS

The number of visible blood vessels within high-power ROIs decreased very rapidly after CA-4-P treatment (Fig. 1, *a* and *b*), the effect being more profound for the 100 mg/kg dose than for the 30 mg/kg dose. After 30 mg/kg CA-4-P (Fig. 1*a*), total visible vessel number decreased to ~65% of the pretreatment number by 10 min after treatment but subsequently recovered to around 80% by 45 min. For 100 mg/kg CA-4-P (Fig. 1*b*), there was a similar initial reduction in total vessel number, but with no indication of recovery at the later times. Reduction in small venule number was more pronounced than reduction in large venule number, especially for the 100 mg/kg group, the difference becoming statistically significant at early times after treatment in this group (Fig. 1*b*). Interestingly, a slight decrease in the total number of vessels over time was observed for untreated tumors (*shaded regions* in Fig. 1, *a* and *b*). However, this was not the case if vessels that were invisible in the pretreatment images, but which appeared in subsequent images, were included in the analysis (data not shown). This is indicative of some temporal fluctuations in the flow in the untreated tumors. A small number of "new" vessels also appeared in the treated tumors after the start of treatment, but inclusion of these did not make a significant difference to the data shown in Fig. 1.

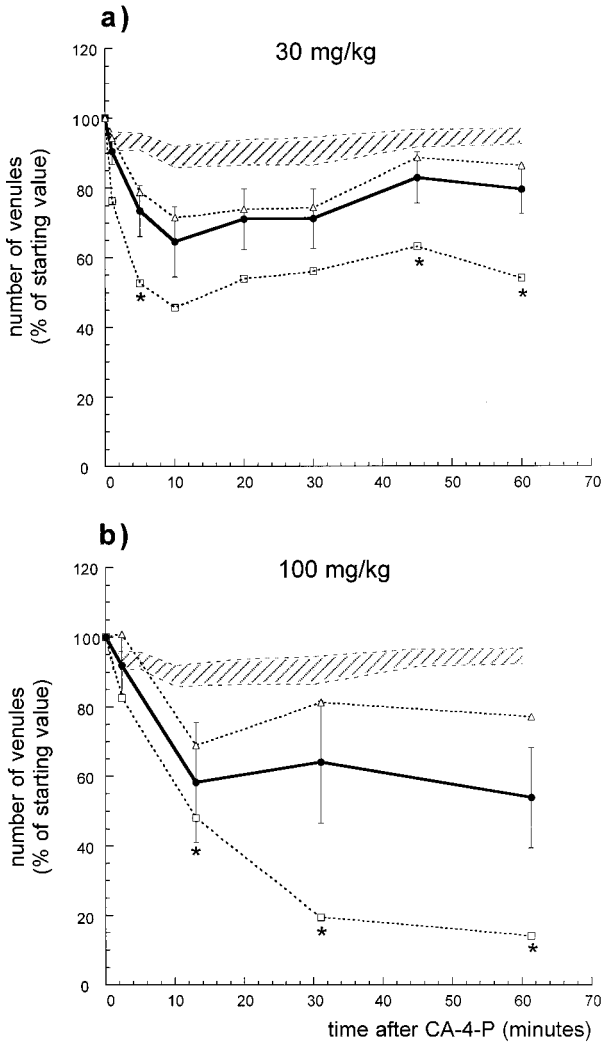

Fig. 1. Effect of different CA-4-P doses on vessel counts in the P22 tumor with time after treatment. Data were obtained by counting venules in pretreatment images (time 0) and then scoring them as present or absent in images at subsequent time points. Venules were counted under visible light, in high-power ROIs (×20 objective) of both upper and lower tumor surfaces, for 1 h after CA-4-P treatment at 30 mg/kg (*a*) or 100 mg/kg (*b*). Data are means ± 1 SE for $n = 12$, average of 33 vessels/tumor for 30 mg/kg; and $n = 5$ to 6, average of 51 vessels/tumor for 100 mg/kg. *Shaded regions* in *a* and *b* indicate means ± 1 SE for tumors in untreated animals ($n = 12$; average of 31 vessels/tumor). Total venules (●) were broken down into small (<10 μm diameter, □) and large (>10 μm diameter, △) venules. Errors are omitted from the data on large and small venules for clarity. ∗ represents significant difference ($P < 0.05$) between large and small venules.

Additional analyses were carried out to investigate the recovery in vessel number observed for 30 mg/kg CA-4-P, and the additional effect of NOS inhibition. Fig. 2 shows that, for venules on the upper surface of tumors, the number of visible vessels, as shown in Fig. 1*a*, is a poor reflection of the functionality of vessels that reappear at later times. Approximately 4% of vessels in untreated tumors were nonfunctioning. The number of nonfunctioning vessels increased with time for rats treated with 30 mg/kg CA-4-P or with the combination of 30 mg/kg CA-4-P and NOS inhibition, with no indication of recovery at later times. There were significantly more nonfunctioning vessels in the combination group than in the CA-4-P alone group at 45 and 60 min post-CA-4-P. However, because L-NNA alone caused some vessels to stop functioning, this effect may be no more than additive (Fig. 2). Nonfunctioning vessels were defined as those which disappeared from the field of view plus those which were visible but contained nonflowing red cells. Therefore, the recovery in total vessel number, as shown in Fig. 1*a*, predominantly consists of this latter group of nonflowing vessels. Presumably, red cells began to reflow in some of the vessels, which had disappeared from view, accounting for the recovery in numbers; but this returned flow was only temporary. By 1 h after the start of CA-4-P, there were two to three times more vessels in the visible, nonflowing category than in the disappeared category for both CA-4-P treatment alone and for the combination with NOS inhibition (data not shown). In the L-NNA group, most of the nonfunctioning vessels were in the disappeared category, for the whole time course. There is no obvious explanation for the difference between the L-NNA group and the combination group before time 0, except that the data are very heterogeneous for the L-NNA group, principally because of a large number of nonfunctioning vessels in one tumor of this group. Venules on the lower surface of tumors responded very similarly to those on the upper surface. Arterioles tended to be more resistant, but this did not reach statistical significance with the number of vessels analyzed (data not shown).

Venules on the upper surface of tumors tended to be narrower and slower-flowing than venules on the lower surface. Mean ± 1 SE for the starting diameters of venules was 10.4 ± 0.5 μm for the upper surface compared with 21.0 ± 2.9 μm for the lower surface. The corresponding red cell velocities were 382 ± 58 μm/s and 870 ± 193 μm/s, respectively. Arteriolar diameter was 14.5 ± 3.2 μm and red cell velocity in arterioles was 3306 ± 235 μm/s. Fig. 3*a* shows the changes in the MABP observed for rats treated with 30 mg/kg CA-4-P alone, L-NNA alone (10 mg/kg plus constant infusion), or the combination of the two agents. MABP was significantly increased for both L-NNA alone and CA-4-P alone; however, the pattern of change was different for the two agents. MABP was significantly raised after L-NNA throughout the whole time course of the experiment, reaching a maximum (150% of the starting value) at ~10 min after the bolus administration. After ~10 min at this pressure, MABP decreased to around 120% of the pretreatment value despite a continuous infusion of L-NNA throughout this period. After CA-4-P treatment, MABP gradually increased to around 125% of the starting value, which was

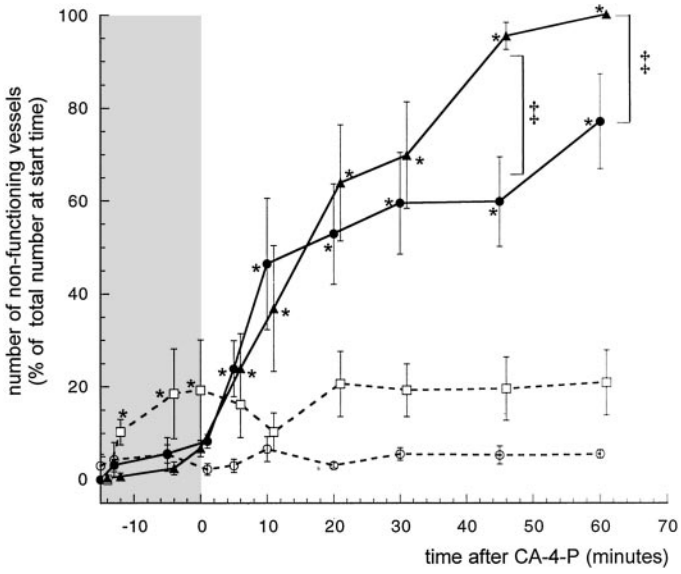

Fig. 2. Effect of different treatments on the percentage of nonfunctioning venules in the P22 tumor with time after treatment. The numbers of nonfunctioning venules, as fractions of the total number of venules at time zero, were counted under visible light in high-power ROIs (×20 objective) of the upper surface of tumors. Vessels were defined as nonfunctional if they had either disappeared from the field of view or if red cells were stationary for at least 30 s. Data are means ± 1 SE for $n = 6$ in each group. Mean number of vessels at time zero was 28–42 in each group. Treatments were 30 mg/kg CA-4-P alone (●), NOS inhibition alone (□), 30 mg/kg CA-4-P plus NOS inhibition (▲); and vehicles only (○). ∗, significant difference ($P < 0.05$) from untreated tumors; ‡, significant difference ($P < 0.05$) between CA-4-P alone and CA-4-P plus NOS inhibition.

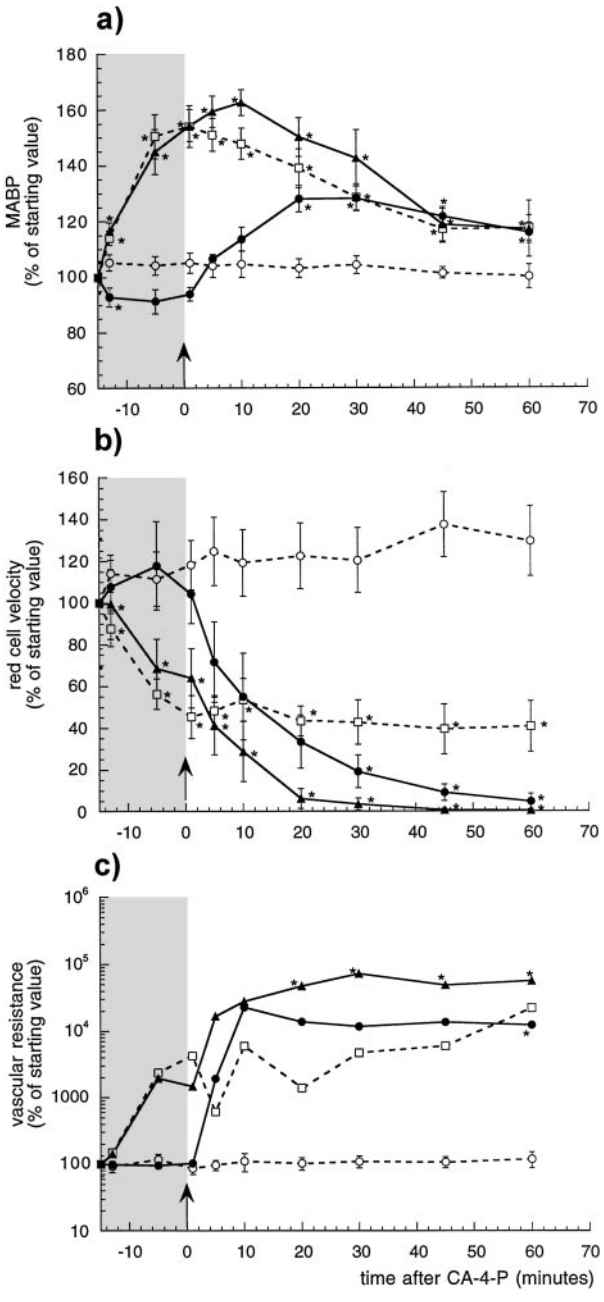

Fig. 3. Effect of different treatments on MABP in tumor-bearing BD9 rats (*a*), tumor red cell velocity (*b*), and tumor vascular resistance (*c*) with time after treatment. Tumor data were evaluated in venules from high-power ROIs of the upper surface of tumors. Red cell velocity was measured by monitoring red cells under fluorescence microscopy. Venular diameters, used for the calculation of relative vascular resistance, were measured under visible light. Data are means ± 1 SE for $n = 5$ in each group. Four vessels analyzed per tumor. For clarity, errors are omitted for treated groups in *c*. Treatments were 30 mg/kg CA-4-P alone (●), NOS inhibition alone (□), 30 mg/kg CA-4-P plus NOS inhibition (▲), and vehicles only (○). ∗, significant difference ($P < 0.05$) from untreated tumors.

maintained throughout the time course of the experiment. These results are consistent with previously reported values for NOS inhibition and CA-4-P (15, 30, 31). The effect of the combination of CA-4-P and L-NNA on MABP was not significantly different from that of L-NNA alone.

Fig. 3*b* shows the changes in red cell velocity within selected tumor blood vessels of the upper surface of tumors within high-power ROIs. The effect of CA-4-P on red cell velocity is extremely rapid, with velocity falling throughout the time course of the experiment and reaching <5% of its starting value by 1 h. This blood flow shut-down is impressive in light of the increase in MABP over the same time course (Fig. 3*a*), which will tend to increase the perfusion pressure of individual vessels and therefore maintain flow. L-NNA caused a significant reduction in red cell velocity almost immediately, reaching a maintained value of 50% by 15 min after bolus administration. The combination treatment is more effective than CA-4-P alone but, as for the data shown in Fig. 2 for the whole tumor field, there is little indication of anything more than an additive effect of the two agents. Similar results were obtained for venules on the lower surface of tumors [preliminary data published previously (19)].

Blood flow rate was calculated from the velocity data shown in Fig. 3*b* and the diameter of the individual vessels. Results were almost identical to those shown for velocity, except that the increase in flow for the control group was smaller than the increase in velocity (data not shown). This similarity reflects the fact that average changes in venule diameter were very minor for all treated groups (Fig. 4), and that blood flow rate in the treated groups was determined predominantly by changes in local perfusion pressures and/or blood viscosity rather than by venular diameters.

Changes in vascular resistance for individual vessels (Fig. 3*c*) were calculated from the MABP data shown in Fig. 3*a* and the blood flow rate data. This calculation assumes that a change in MABP produces an identical change in perfusion pressure in all of the individual vessels analyzed. Although this is unlikely to be the case, and the resulting values are very variable for the treated groups (see legend to Fig. 3), the data do indicate that vascular resistance is greatly increased after treatment with CA-4-P or the combination of CA-4-P with L-NNA. In addition, the calculated vascular resistance for the control group was almost constant with time (Fig. 3*c*), in contrast to velocity and flow, which significantly increased. This is attributable to a balancing effect of the increase in MABP and the increase in flow rate for individual vessels in this group.

There was a tendency for hematocrit to increase in the larger venules analyzed on the lower surface of the tumors after treatment with CA-4-P, which reached significance at 10 min posttreatment but not at 20 min (data not shown). Fig. 4 shows the effects of the different treatments on vessel diameter. There is a small but significant reduction in arteriole diameter at 45 and 60 min after CA-4-P treatment, but there is no significant effect on the venules (Fig. 4, *a* and *b*, respectively). L-NNA caused a significant reduction in arteriolar diameter to ~80% of control, but this was lost at later times (Fig. 4*c*). No significant effects were found for venules (Fig. 4*d*). This result is similar to previously published data for this agent (32). For the combination treatment, there was a progressive and profound reduction in arteriolar diameter, which reached ~60% of control by 45 min (Fig. 4*e*). There was also an early significant but smaller reduction in the diameter of venules to ~85% of control, but these vessels recovered at later times, with some vessels dilating beyond their starting values (Fig. 4*f*). A similar response pattern was seen for both CA-4-P and the combination treatment in the venules of the upper surface (Fig. 5). It is apparent that the pattern of response to CA-4-P or the combination treatment is different for arterioles and venules, with arterioles tending to show a sustained reduction in diameter, and venules tending to recover from any decrease, at later times. Some venules, but not arterioles, seemed to be dilated compared with their starting values (Fig. 4, *a*, *b*, *e*, and *f*; and Fig. 5).

Fig. 5 shows example images from video records of tumors from rats at different times after treatment. These images illustrate the decrease in number of visible vessels with time after treatment with CA-4-P or CA-4-P combined with L-NNA and then a partial recovery at later times, as quantified in Fig. 1*a*. It also shows that most of the

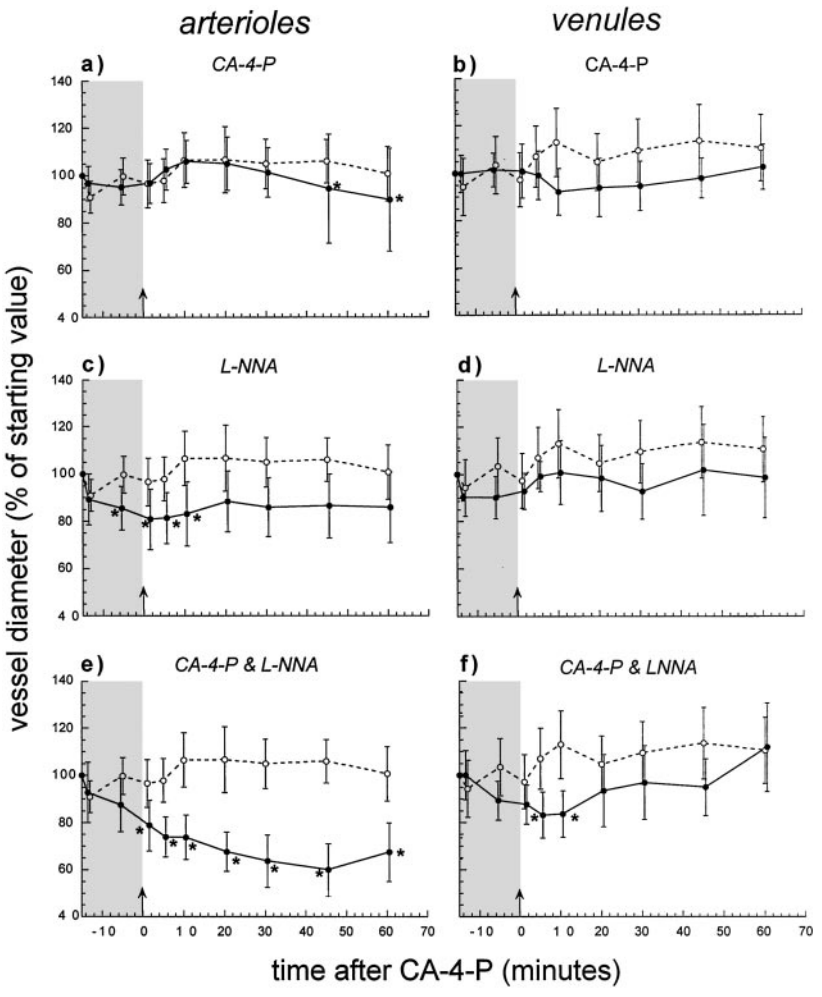

Fig. 4. Effect of different treatments on diameter of large venules and arterioles of the P22 tumor with time after treatment. Data are for blood vessels from high-power ROIs of the lower tumor surface after 30 mg/kg CA-4-P alone [arterioles (*a*) and venules (*b*)]; NOS inhibition alone [arterioles (*c*) and venules (*d*)]; 30 mg/kg CA-4-P plus NOS inhibition [arterioles (*e*) and venules (*f*)]. Data are means ± 1 SE for $n = 4-6$ in each group. One to 4 vessels analyzed per tumor. (○), vehicle; (●), treated. ∗, significant difference ($P < 0.05$) from untreated tumors.

vessel loss is in the center of tumors. An increase in diameter of some of the larger venules, by the end of the observation time, is also apparent, especially for the combination treatment. Other observations, which were not quantified, are illustrated in Fig. 5. First, a general darkening at the tumor periphery was apparent for the CA-4-P- and CA-4-P-plus-L-NNA-treated tumors at the later times. This is most likely attributable to hemorrhage from the peripheral vessels. Difficulty in focusing the ×40 objective was noted in a majority of treated tumors, starting at early times after treatment; and this may also be related to an increased permeability of tumor venules, resulting in edema. Red cell stacking (formation of rouleaux), as blood flow slowed, was very apparent and is illustrated in Fig. 5. Recordings were made of the granulation tissue surrounding tumors at the start and finish of the observation period. It was obvious that blood flow was reduced in this tissue by CA-4-P and the combination treatment, although the effect was not as profound as in the tumor tissue. On a few occasions, the visible tumor vasculature in the high-power ROI or in a larger area completely disappeared for a few seconds. Presumably, this is attributable to a temporary shut-down of a supplying vessel or vessels upstream from the ROI.

Fig. 6 shows the effect of CA-4-P on the uptake of BSA into the P22 tumor. The tumor uptake index for ^{125}I albumin/^{86}RbCl was significantly increased by ~60% at 1 and 10 min after CA-4-P treatment compared with control values. This indicates a significant increase in tumor vascular permeability to albumin at early times after treatment.

DISCUSSION

These results demonstrate graphically an extensive and very rapid shut-down in tumor blood flow after systemic treatment of rats with CA-4-P. After a dose of 30 mg/kg, blood flow rate to the center of P22 tumors was <5% of the starting value within minutes of i.p. administration and was almost zero by 1 h. Analysis of the number of visible vessels showed a different response for 30 and 100 mg/kg CA-4-P. Numbers recovered at later times for the lower dose but not for the higher dose. Although blood did not continue to flow in these returning vessels for the 1-h time course of this experiment (Fig. 2), the difference between the two doses may be predictive of a later recovery in flow. Indeed, using a radiotracer method, there was no recovery of blood flow rate in subcutaneously transplanted P22 tumors at 6 h after 100 mg/kg CA-4-P (15). At 24 h, there was a partial recovery for 30 mg/kg CA-4-P but not for 100 mg/kg.[4]

Very small venules accounted for most of the disappeared tumor blood vessels after CA-4-P treatment. It is not clear whether these vessels collapsed completely or whether they collapsed/constricted or became blocked with red cells locally, which allowed the downstream passage of plasma but not red cells. Because vessels could only be identified under visible light by the presence of red cells, we could not distinguish between these events. Attempts to label the plasma with TRITC-albumin for identification of vessels under fluorescence

[4] V. E. Prise, J. Wilson, D.J. Honess, and G. M. Tozer. Blood flow response of tumors and normal tissues to treatment with combretastatin A-4-P, manuscript in preparation.

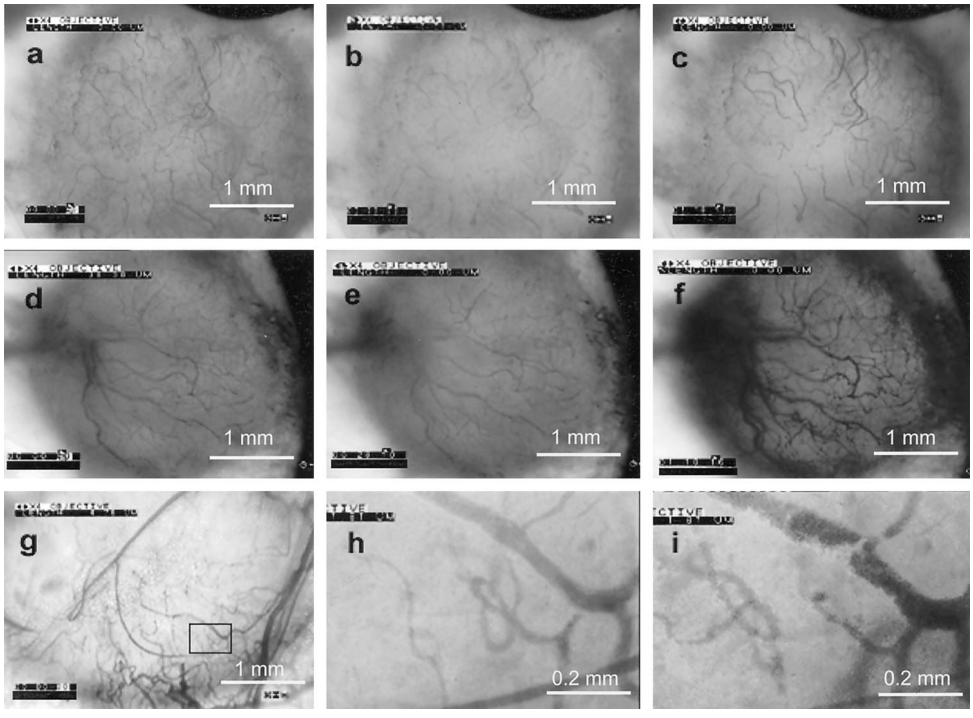

Fig. 5. Example images, taken under visible light conditions, of tumors from rats treated with CA-4-P alone (*a*, *b*, and *c*) and CA-4-P plus NOS inhibition (*d*, *e*, *f*, *g*, *h*, and *i*). Images on the *left* (*a*, *d*, and *g*) and image *h*, tumors before treatment. *Middle*, *top two rows* (*b* and *e*), tumors 10–20 min after the start of treatment. Images on the *right* (*c*, *f*, and *i*), tumors at the end of the observation period (60 min after start of treatment). Images *a*–*g* were obtained using a ×4 objective. Images *h* and *i* were obtained using a ×20 objective. Images *h* and *i* represent an ROI taken approximately from the rectangle shown in *g*. *Top two rows*, the upper surface of tumors. *Third row*, the lower surface of a tumor, where larger, draining venules are clearly visible. The images show the disappearance of a large number of venules at early times after treatment and then a return of the visible vasculature at later times. Many venules are clearly distended/dilated at the end of the observation period (*c* and *f*). *h* and *i*, the development of rouleaux in a large venule, caused by the stacking of red cells, with time after treatment.

conditions were inconclusive because of leakage from the vessels (data not shown). A very small decrease in diameter of a small venule would close it off completely. This could occur via various means. First, the observed increase in tumor vascular permeability to plasma proteins could result in a net transport of water from the plasma into the interstitial space (edema), resulting in an imbalance between the intravascular and tissue hydrostatic pressures, causing vascular collapse. Second, a decrease in diameter could be caused by the rounding-up of endothelial cells, an effect consistently observed after exposure of endothelial cells in culture to low concentrations of CA-4-P (13, 18, 19). A third possibility, that leukocyte adherence to the vascular wall could account for changes in venular diameter (33), is unlikely because, in an *in vitro* flow system, neutrophil adherence to an endothelial cell monolayer was only observed after several hours' exposure to CA-4-P (34). In addition, a very rapid increase in vascular resistance of P22 tumors was observed after exposure to CA-4-P in an isolated perfusion system where leukocytes were absent (15). Some venules were obviously widened and engorged with red cells by the end of treatment, an effect which was most profound in tumors from rats treated with the combination treatment (Fig. 5). This suggests some recovery from the initial effects of CA-4-P combined with local increases in intravascular pressures, perhaps caused by continued down-stream vessel narrowing, which caused the vessels to distend. Using conventional histology, the widening and engorgement of venules in the P22 tumor were not commonly associated with coagulation at those times.[5]

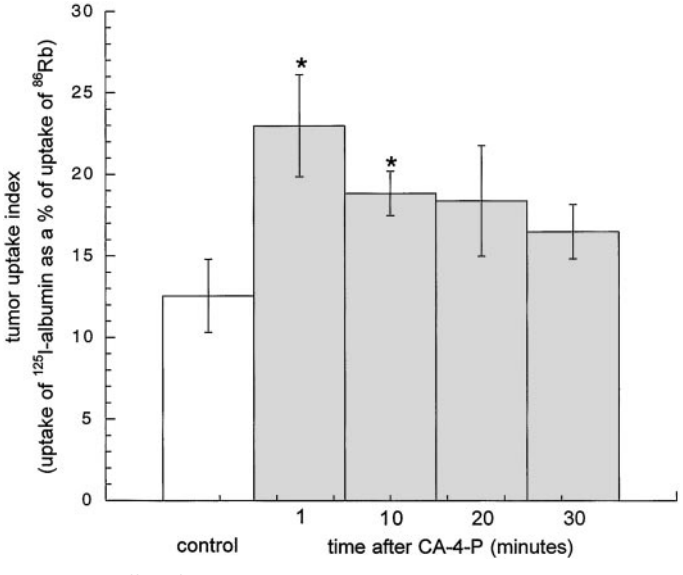

Fig. 6. The effect of 30 mg/kg CA-4-P on tumor vascular permeability to albumin at various times after i.p. administration of the drug as measured by calculation of a tumor uptake index for ^{125}I-labeled BSA (see text for details). Data are means ± 1 SE for $n = 7$ to 10. ∗, a significant difference from control ($P < 0.05$).

Diameter changes in venules are unlikely to be caused by active vasoconstriction/vasodilation, especially as the pattern of change in venule diameter after treatment was very different from those observed in arterioles (Fig. 4). The reduction in arteriolar diameter to ~80% of the starting value by 15 min after administration of L-NNA alone is consistent with reported values for other tumors (32). Arteriolar vasoconstriction (or, strictly, reversal of vasodilation) could account for all of the flow reduction observed for L-NNA alone, and this is consistent with the absence of any changes in vessel numbers, hematocrit, or rheology in the current study. That is, blood flow rate is proportional to the fourth power of vessel radius (Poisseuille's law; Ref. 35). This means that a reduction in arteriolar radius to 80% would reduce flow rate through the system to 41%, which is very close to the actual data for red cell velocity (Fig. 3*b*) and blood flow rate (data not shown). For the group treated with CA-4-P alone, there was no reduction in arteriolar or venular diameter at early times, which could account for the profound blood flow reduction observed in these tumors (comparing Fig. 4, *a* and *b*, with Fig. 3*b*). The small arteriolar constriction, to ~90% of the starting value, at 1 h posttreatment (Fig. 4*a*), would contribute to the maintenance of blood flow reduction at this time, but it is only sufficient to reduce blood flow to 66% of the

[5] G. M. Tozer and V. E. Prise, unpublished data.

starting value (Poisseuille's law). Clearly, this does not account for the full effect of the drug. The combination treatment produced a profound effect on arteriolar diameter, reducing it to ~60% of the starting value by 45 min after the start of CA-4-P treatment. However, even this major vasoconstriction is only sufficient to reduce blood flow rate to 13% of the starting value, which clearly is not sufficient to account for the changes shown in Fig. 3.

The increase in vascular permeability to albumin, observed in the inguinal fat pad tumors at 1 and 10 min after CA-4-P treatment, is likely to be a key factor leading to blood flow shut-down. This could occur not only via physical collapse of a subpopulation of small venules (see above) but also via an increase in intravascular hematocrit, leading to an increase in blood viscosity consequent to fluid loss from the vasculature. Indeed, there was some evidence for an increased hematocrit in large venules of the lower tumor surface at early times after treatment. In the rat, vascular shut-down by CA-4-P is specific for tumors, with most normal tissues minimally affected by the drug (15). It will be important to determine whether this is attributable to the absence of permeability changes in normal tissue blood vessels after CA-4-P, or whether blood flow in normal tissues can be sustained in the face of increases in permeability. This study is currently under way. An increase in blood viscosity could also be caused by any direct effect of CA-4-P on red cell shape, but this has not been investigated. It has been suggested that small changes in red cell deformability may occur more readily and have a greater consequence in tumors than in normal tissues because of the unique tumor metabolic environment and vascular morphology (36).

The behavior of red cells at low flow rates *in vivo* has been described recently (37). It was found that, below a critical red cell velocity (250 to 300 μm/s), red cell movement became erratic, with significant radial movements away from the main direction of flow. This was associated with orientation changes involving the long axis of the cell becoming rather perpendicular to the direction of flow. These conditions lead to an energy dissipation of flow and an enhanced collisions of red cells with each other. This, in turn, leads to the stacking of red cells to form rouleaux and a massive increase in viscosity and vascular resistance to flow. Rouleaux may completely block microvessels. Mean pretreatment velocities in venules of the upper surface of tumors were ~500 μm/s, and rouleaux formation was consistently observed as flow rates decreased after CA-4-P treatment. Thus, these rheological changes are likely to play a major part in the vascular shut-down observed in the current study, and there will be a positive feed-back, with blood flow reduction leading to the stacking behavior, which leads to additional blood flow reduction. In addition, as blood flow reduces, the tumor blood vessels will become more hypoxic, and this can increase the suspension viscosity of red cells (38) and increase rouleaux formation, the latter via exposure of adhesion molecules on the surface of the cells. This may be more apparent in the central vessels, which tend to be more hypoxic than the peripheral ones (39, 40). A summary of the putative mechanisms leading from CA-4-P-induced damage to the vascular endothelium to blood flow collapse is shown in Fig. 7 and is reminiscent of an acute inflammatory reaction.

We propose that part of the selectivity of CA-4-P for tumor tissue, which has been demonstrated previously (15), is attributable to the spatial heterogeneity in tumor blood flow. Many tumor vessels have sluggish flow, which is variable over time, and these vessels will be particularly susceptible to CA-4-P. Other possibilities center around differences between tumor and normal tissue endothelial cells, which would affect the primary damage inflicted on these cells. These include differences in proliferation rate (10), posttranslational modifications of tubulin, interaction between the tubulin and actin cytoskeletons, and microenvironmental factors such as oxygenation and

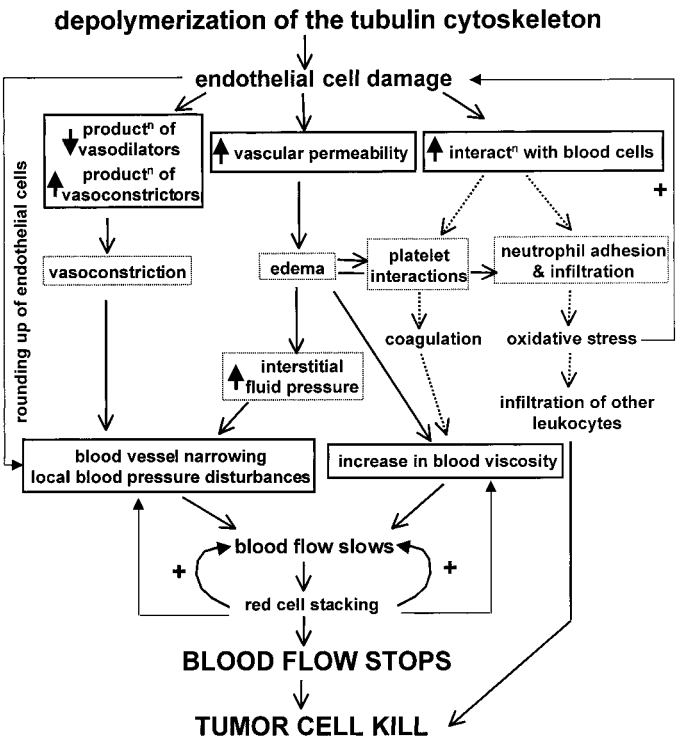

Fig. 7. Potential mechanisms for the shut-down in tumor blood flow after systemic treatment with CA-4-P. CA-4-P causes depolymerization of the tubulin cytoskeleton in endothelial cells *in vitro*, leading to endothelial cell damage and shape changes. *In vivo*, a rounding-up of endothelial cells could lead directly to a narrowing of tumor blood vessels. Alternately, blood flow could be influenced by functional changes in endothelial cells; the main functions being production of vasoactive agents, control of solute transport between tissue and blood (vascular permeability), and involvement in immunological/inflammatory processes via interaction with blood cells. Disturbances in these functions would lead to a decrease in blood flow via alterations in local perfusion pressures (blood pressure disturbances), geometric resistance to flow (especially blood vessel narrowing), and viscous resistance to flow (blood viscosity), via the mechanisms shown. The current data indicate a relatively minor role for the altered production of vasoactive agents in this pathway. Endothelial-blood cell interactions are likely to be important but cannot explain the very early effects of the drug (*dashed arrows*). An increase in vascular permeability to macromolecules is likely to be an important early event leading to edema, expression of adhesion molecules, an increase in interstitial fluid pressure, and an increase in blood viscosity. Initial blood flow reduction will cause red cell stacking (rouleaux formation), which will positively feed back to additional blood flow reduction via a catastrophic increase in blood viscosity. See text for details.

NO production. It is also possible that the "mature" vasculature of normal tissues can sustain more endothelial cell injury without vascular collapse than can the "immature" vasculature of tumors. Although not the focus of the current study, the immature granulation tissue, which forms the background "normal" tissue of the window chamber tumors, was also affected by CA-4-P, although not as profoundly as the tumor tissue.

Blood flow at the periphery of tumors was consistently less affected than at the center of tumors, and this is consistent with the sparing of the tumor periphery in terms of tumor cell toxicity (10). Vessels at the periphery may be more resistant to the primary damage induced by CA-4-P than those at the center as a result of putative differences in vascular/endothelial structure between the two compartments. Alternatively, the peripheral vasculature may be more resistant to some of the secondary effects of CA-4-P treatment. For instance, the peripheral vessels tend to be larger and faster flowing than the central vessels, which would make them less susceptible to blood flow collapse via diameter changes and would make a small blood flow reduction less catastrophic. Similarly, the interstitial fluid pressure of tumors tends to drop precipitously at the tumor periphery (41), and this would favor vascular collapse in the central region. The fact that hemorrhage was apparent at the periphery of tumors after CA-4-P

treatment is an indication that the peripheral vessels may be just as sensitive to the primary effects of CA-4-P as the central vessels. Whatever the cause, it is apparent that the reduced response of the peripheral vessels limits the effectiveness of CA-4-P and causes rapid regrowth of tumors after treatment. Combination of CA-4-P with treatments designed specifically to target the tumor cells in the periphery have shown particular promise (42).

The effect of acute systemic NOS inhibition, using L-NNA, was to decrease red cell velocity and blood flow rate by 50% throughout the observation period, which is consistent with previous studies for this tumor growing s.c. (31). Similar results have been reported for other tumors (32). There was significant arteriolar vasoconstriction, which would account for the blood flow changes induced by L-NNA alone. An increase in leukocyte-endothelial interactions is also a likely consequence of NOS inhibition (32), although this was not investigated in the current study. NO is known to influence vascular permeability, although its effects in tumors are variable. Fukumura *et al.*, (32) found that systemic NOS inhibition reduced vascular permeability to albumin in one experimental tumor model but not in a second. A reduction in tumor vascular permeability after the administration of L-NNA would tend to protect against vascular damage by CA-4-P, if our hypothesis regarding the role of vascular permeability changes in CA-4-P-induced vascular damage is correct. Clearly this was not the case, indicating that additional experiments are required to clarify potential interactions between NOS inhibition and CA-4-P.

Qualitatively, the vascular effects of L-NNA alone were very different from those of CA-4-P alone, arteriolar vasoconstriction playing only a minor part in the latter case, as described above. The vascular effects of the combination of L-NNA with CA-4-P were qualitatively very similar to those for CA-4-P alone, but the effects were greater for the combined-treatment group. At the end of the observation period, vascular resistance seemed to be higher, and there were more stagnant, distended vessels in the combined-treatment group than in the CA-4-P-alone group. However, there was no evidence for a potentiating effect of L-NNA on CA-4-P, which was found previously for the prodrug of L-NNA, N$^{\omega}$-nitro-L-arginine methyl ester, on tumor blood flow and vascular resistance in the P22 tumor grown s.c. (15). There could be several reasons for this disparity relating to the differences in experimental design, and this requires additional investigation. In any case, the current study reveals that CA-4-P induces a reduction in tumor blood flow, which is qualitatively different from that obtained with NOS inhibition, and it suggests that the combination of the two approaches may be advantageous. Tumor growth and toxicity studies are required to test this possibility.

In conclusion, this paper describes the tumor vascular response to systemic treatment with CA-4-P and suggests a mechanism of action leading from initial tubulin binding to vascular shut-down. This mechanism is reminiscent of a classical acute inflammatory reaction, involving a very rapid increase in vascular permeability to plasma proteins. It suggests that acute NOS inhibition, in combination with CA-4-P treatment, has an additive effect that may be possible to exploit therapeutically. CA-4-P is now in clinical trial as one of the few primarily antivascular, as opposed to antiangiogenic, drugs currently available. It will be important to fully elucidate its mechanism of action to be able to use it effectively and to develop this approach further.

ACKNOWLEDGMENTS

We thank the Gray Cancer Institute, Northwood, United Kingdom, staff for care of the animals. We are indebted to Dr. Vincent Cunningham and John Aston, Imaging Research Solutions Ltd., London, United Kingdom, for their contribution to the statistical analysis. We thank the Cancer Research Campaign, the National Lottery Charities Board of the United Kingdom, and NATO for funding this work; and OxiGene, Inc. for kindly supplying the CA-4-P.

REFERENCES

1. Folkman, J. Angiogenesis and angiogenesis inhibition: an overview. *In:* I. D. Goldberg and E. R. Rosen (eds.), Regulation of Angiogenesis, pp. 1–8. Basel: Birkhäuser Verlag, 1997.
2. Chaplin, D. J., and Dougherty, G. J. Tumor vasculature as a target for cancer therapy. Br. J. Cancer, *80* (Suppl. 1)*:* 57–64, 1999.
3. Chaplin, D. J., Pettit, G. R., Parkins, C. S., and Hill, S. A. Antivascular approaches to solid tumor therapy: evaluation of tubulin binding agents. Br. J. Cancer, *74* (Suppl. XXVII)*:* S86–S88, 1996.
4. Baguley, B. C., Zhuang, L., and Kestell, P. Increased plasma serotonin following treatment with flavone-8-acetic acid, 5,6-dimethylxanthenone-4-acetic acid, vinblastine, and colchicine: relation to vascular effects. Oncol. Res., *9:* 55–60, 1997.
5. Hill, S. A., Lonergan, S. J., Denekamp, J., and Chaplin, D. J. Vinca alkaloids: anti-vascular effects in a murine tumor. Eur. J. Cancer, *29A:* 1320–1324, 1993.
6. Seed, L., Slaughter, D. P., and Limarzi, L. R. Effect of colchicine on human carcinoma. Surgery, *7:* 696–709, 1940.
7. Pettit, G. R., Singh, S. B., Hamel, E., Lin, C. M., Alberts, D. S., and Garia-Kendall, D. Isolation and structure of the strong cell growth and tubulin inhibitor combretastatin A4. Experientia, *45:* 205–211, 1989.
8. Pettit, G. R., Temple, C., Narayanan, V. L., Varma, R., Simpson, M. J., Boyd, M. R., Rener, G. A., and Bansal, N. Antineoplastic agents 322. Synthesis of combretastatin A-4 prodrugs. Anticancer Drug Des., *10:* 299–309, 1995.
9. Woods, J. A., Hadfield, J. A., Pettit, G. R., Fox, B. W., and McGown, A. T. The interaction with tubulin of a series of stilbenes based on combretastatin A-4. Br. J. Cancer, *71:* 705–711, 1995.
10. Dark, G. D., Hill, S. A., Prise, V. E., Tozer, G. M., Pettit, G. R., and Chaplin, D. J. Combretastatin A-4, an agent that displays potent and selective toxicity toward tumor vasculature. Cancer Res., *57:* 1829–1834, 1997.
11. Beauregard, D. A., Thelwall, P. E., Chaplin, D. J., Hill, S. A., Adams, G. E., and Brindle, K. M. Magnetic resonance imaging and spectroscopy of combretastain A_4 prodrug-induced disruption of tumor perfusion and energetic status. Br. J. Cancer, *77:* 1761–1767, 1998.
12. Horsman, M., Ehrnrooth, E., Ladekarl, M., and Overgaard, J. The effect of combretastatin A-4 disodium phosphate in a C3H mouse mammary carcinoma and a variety of murine spontaneous tumors. Int. J. Radiat. Oncol. Biol. Phys., *42:* 895–898, 1998.
13. Grosios, K., Holwell, S. E., McGown, A. T., Pettit, G. R., and Bibby, M. C. *In vivo* and *in vitro* evaluation of combretastatin A-4 and its sodium phosphate prodrug. Br. J. Cancer, *81:* 1318–1327, 1999.
14. Chaplin, D. J., Pettit, G. R., and Hill, S. A. Anti-vascular approaches to solid tumor therapy: evaluation of combretastatin A4 phosphate. Anticancer Res., *19:* 189–196, 1999.
15. Tozer, G. M., Prise, V. E., Wilson, J., Locke, R. J., Vojnovic, B., Stratford, M. R. L., Dennis, M. F., and Chaplin, D. J. Combretastatin A-4 phosphate as a tumor vascular-targeting agent: early effects in tumors and normal tissues. Cancer Res., *59:* 1626–1634, 1999.
16. Parkins, C. S., Dennis, M. F., Stratford, M. R. L., Hill, S. A., and Chaplin, D. J. Ischemia reperfusion injury in tumors: the role of oxygen radicals and nitric oxide. Cancer Res., *55:* 6026–6029, 1995.
17. Korbelik, M., Parkins, C. S., Shibuya, H., Cecic, I., Stratford, M. R., and Chaplin, D. J. Nitric oxide production by tumor tissue: impact on the response to photodynamic therapy. Br. J. Cancer, *82:* 1835–1843, 2000.
18. Kanthou, C., and Tozer, G. M. Studies on the mechanism of action of the vascular targeting agent combretastatin A-4 phosphate. Br. J. Cancer, *83* (Suppl. 1)*:* 12, 2000.
19. Galbraith, S. M., Chaplin, D. J., Lee, F., Stratford, M. R. L., Locke, R. J., Vojnovic, B., and Tozer, G. M. Effects of combretastatin A4 phosphate on endothelial cell morphology *in vitro* and relationship to tumor vascular targeting activity *in vivo*. Anticancer Res., *21:* 93–102, 2001.
20. Li, L., Rojiani, A., and Siemann, D. Targeting the tumor vasculature with combretastatin A-4 disodium phosphate: effects on radiation therapy. Int. J. Radiat. Oncol. Biol. Phys., *42:* 899–903, 1998.
21. Grosios, K., Loadman, P. M., Swaine, D. J., Pettit, G. R., and Bibby, M. C. Combination chemotherapy with combretastatin A-4 phosphate and 5-fluorouracil in an experimental murine colon adenocarcinoma. Anticancer Res., *20:* 229–234, 2000.
22. Papenfuss, H. D., Gross, J. F., Intaglietta, M., and Treese, F. A. A transparent access chamber for the rat dorsal skin fold. Microvasc. Res., *18:* 311–318, 1979.
23. Dewhirst, M. W., Gustafson, C., Gross, J. F., and Tso, C. Y. Temporal effects of 5.0 Gy radiation in healing subcutaneous microvasculature of a dorsal flap window chamber. Radiat. Res., *112:* 581–591, 1987.
24. Tozer, G. M., and Shaffi, K. M. Modification of tumor blood flow using the hypertensive agent, angiotensin II. Br. J. Cancer, *67:* 981–988, 1993.
25. Unthank, J., Lash, J., Nixon, J., Sidner, R., and Bohlen, H. Evaluation of carbocyanine-labeled erythrocytes for microvascular measurements. Microvasc. Res., *45:* 193–210, 1993.
26. Kimura, K., Braun, R. D., Ong, E. T., Hsu, R., Secomb, T. W., Papahadjopoulos, D., Hong, K., and Dewhirst, M. W. Fluctuations in red cell flux in tumor microvessels can lead to transient hypoxia and reoxygenation in tumor parenchyma. Cancer Res., *56:* 5522–5528, 1996.
27. Gonzalez, R. C., and Woods, R. E. Digital Image Processing. Reading, MA: Addison-Wesley Publishing Co., 1993.

28. Tozer, G. M., Shaffi, K. M., Prise, V. E., and Cunningham, V. J. Characterisation of tumor blood flow using a "tissue-isolated" preparation. Br. J. Cancer, *70:* 1040–1046, 1994.
29. Oldendorf, W. H. Measurement of brain uptake of radiolabelled substances using a tritiated water internal standard. Brain Res., *24:* 372–376, 1970.
30. Rees, D. D., Palmer, R. M. J., Schulz, R., Hodson, H. F., and Moncada, S. Characterization of three inhibitors of endothelial nitric oxide synthase *in vitro* and *in vivo*. Br. J. Pharmacol., *101:* 746–752, 1990.
31. Tozer, G. M., Prise, V. E., and Chaplin, D. J. Inhibition of nitric oxide synthase induces a selective reduction in tumor blood flow that is reversible with L-arginine. Cancer Res., *57:* 948–955, 1997.
32. Fukumura, D., Yuan, F., Endo, M., and Jain, R. K. Role of nitric oxide in tumor microcirculation: blood flow, vascular permeability, and leukocyte-endothelial interactions. Am. J. Pathol., *150:* 713–725, 1997.
33. Parkins, C. S., Holder, A. J., Hill, S. A., Chaplin, D. J., and Tozer, G. M. Determinants of anti-vascular action by combretastatin A-4 phosphate: role of nitric oxide. Br. J. Cancer, *83:* 811–816, 2000.
34. Brooks, A. C., Nash, G. E., Parkins, C. S., and Tozer, G. M. Combretastatin A-4-phosphate (CA-4-P) induces neutrophil recruitment to cultured endothelial cells under flow. J. Vasc. Res., in press, 2001.
35. Levick, J. R. An Introduction to Cardiovascular Physiology. Oxford: Butterworth Heinemann, 1992.
36. Sevick, E. M., and Jain, R. K. Effect of red blood cell rigidity on tumor blood flow: increase in viscous resistance during hyperglycemia. Cancer Res., *51:* 2727–2730, 1991.
37. Lominadze, D., and Mchedlishvili, G. Red blood cell behavior at low flow rate in microvessels. Microvasc. Res., *58:* 187–189, 1999.
38. Kavanagh, B., Coffey, B., Needham, D., Hochmuth, R., and Dewhirst, M. The effect of flunarizine on erythrocyte suspension viscosity under conditions of extreme hypoxia, low pH and lactate treatment. Br. J. Cancer, *67:* 734–741, 1993.
39. Dewhirst, M. W., Ong, E. T., Klitzman, B., Secomb, T. W., Vinuya, R. Z., Dodge, R., Brizel, D., and Gross, J. F. Perivascular oxygen tensions in a transplantable mammary tumor growing in a dorsal flap window chamber. Radiat. Res., *130:* 171–182, 1992.
40. Dewhirst, M., Ong, E., Braun, R., Smith, B., Klitzman, B., Evans, S., and Wilson, D. Quantification of longitudinal tissue pO_2 gradients in window chamber tumors: impact on tumor hypoxia. Br. J. Cancer, *79:* 1717–1722, 1999.
41. Boucher, Y., Baxter, L. T., and Jain, R. K. Interstitial pressure gradients in tissue-isolated and subcutaneous tumors: implications for therapy. Cancer Res., *50:* 4478–4484, 1990.
42. Pedley, R. B., Hill, S. A., Boxer, G. M., Flynn, A. A., Boden, R., Watson, R., Dearling, J., Chaplin, D. J., and Begent, R. H. Eradication of colorectal xenografts by combined radioimmunotherapy and combretastatin A-4 3-O-phosphate. Cancer Res., *61:* 4716–4722.